Research Article Vol. 2, No. 7 / 15 July 2019 / OSA Continuum 2123

Temperature sensor based on liquid-filled negative curvature optical fibers

CHENGLI WEI,[1] JOSHUA T. YOUNG,[1] CURTIS R. MENYUK,[2] AND JONATHAN HU[1,*]

[1]Department of Electrical and Computer Engineering, Baylor University, Waco, TX 76798, USA
[2]Department of Computer Science and Electrical Engineering, University of Maryland Baltimore County, Baltimore, MD 21227, USA
[*]jonathan_hu@baylor.edu

Abstract: We computationally investigate a novel temperature sensor that uses liquid-filled negative curvature optical fibers. Both the core and cladding tubes are infiltrated with a liquid that has a temperature-sensitive refractive index. The high-loss resonant wavelengths are sensitive to the liquid's change of the refractive index. The refractive index of the liquid decreases and the resonant wavelengths increase when the temperature increases. The temperature sensitivity is 1.1 nm/ °C as the temperature changes from 15 °C to 35 °C using negative curvature optical fibers that are filled with liquid that has a refractive index of 1.36. The temperature sensitivity rises from 0.82 nm/ °C to 2.48 nm/ °C when different liquids are used with a refractive index from 1.30 to 1.42, and we use the third resonant peak in the fiber. The temperature sensitivity can be increased by 38% by using the second resonant peak. An analytical formula for the temperature sensitivity is derived, which can give an accurate prediction for the temperature sensitivity of this sensor. The relatively large size of the air core and cladding tubes, on the order of 10 μm, should make the infiltration procedure easier compared to other photonic crystal fibers with smaller holes. With temperature sensors based on liquid-filled negative curvature optical fibers, there is no need for any special post-processing, such as the liquid filling of selected air holes or inscription of fiber gratings.

1. Introduction

Fiber temperature sensors have been widely applied in civil, industrial, and military fields due to their immunity to electromagnetic interference, suitability for remote sensing, chemical inertness, light weight, compact size, high sensitivity, and broad bandwidth [1–3]. Different strategies have been used to construct fiber sensors. Using a bandgap fiber with a high-index liquid in the cladding holes, the temperature can be determined using the bandgap shift when the refractive index of the liquid changes due to the change in temperature [4]. Interferometers can be combined with liquid-filled photonic crystal fibers to make a temperature sensor [5–9]. In interferometer-based fiber sensors, light is first coupled in the core and cladding regions, after which the core and cladding modes propagate while interfering with each other. The interference between the core and cladding modes makes it possible to track temperature changes [8,9]. Long period gratings (LPGs) that are inscribed on liquid-filled photonic crystal fibers can also be used to make temperature sensors. The coupling between the mode in the core and the mode in the cladding will lead to a different resonant wavelength due to the change of the liquid index when the temperature changes [10,11].

The development of air-core optical fibers makes it possible to infiltrate a temperature-sensitive liquid into the fiber and to produce a fiber with a strong overlap between the liquid and the optical modes in the fiber. Liquid-filled hollow-core fibers have been fabricated [12,13]. To fill the holes with liquid, one end of the fiber must be immersed in the liquid. Negative pressure is applied at the other end of the fiber until the air holes are filled. After that, both ends of the

#359757 https://doi.org/10.1364/OSAC.2.002123
Journal © 2019 Received 4 Mar 2019; revised 15 May 2019; accepted 2 Jun 2019; published 24 Jun 2019

OSA CONTINUUM

liquid-filled fiber are spliced to solid-core fibers to form an integrated all-fiber device [14]. In addition, selectively filled photonic crystal fibers can induce resonant coupling between the mode in the high-index liquid and the mode in the core. This resonant coupling is very sensitive to the change of temperature, which can be used to make temperature sensors with a high sensitivity [2,15,16]. However, this selective filling process is time-consuming and difficult due to the small core size and hole size in the cladding [17,18].

Negative curvature air-core optical fibers have attracted a large amount of attention because they make it possible to simultaneously obtain a low loss and a broad transmission band [19–26]. The guiding mechanism of this fiber is inhibited coupling [21,27]. The structure of these fibers is usually simple, and the typical size of the air holes is much larger than is usually the case in bandgap fibers. The process of liquid infiltration into the core of a negative curvature optical fiber that typically has a hole size from 50 μm to 100 μm is expected to be easier than infiltrating a liquid into bandgap fibers, where the hole size is typically less than 10 μm. In this work, we computationally study a novel temperature sensor based on a negative curvature optical fiber that is completely filled with a liquid that is sensitive to temperature changes. The resonant condition will change due to the change of the liquid's index of refraction that is induced by the temperature variation. Therefore, the resonant peak can be used to track the change of temperature. In this fiber sensor, there is no need for complicated device fabrication, such as grating inscription, and there is no need for liquid filling of selected air holes. The infiltration procedure is also relatively simple and efficient [25,28,29]. This work extends earlier work that appeared in [30], in which we presented simulation results. In this work, we describe in greater detail our computational procedures, we derive an analytical result for the temperature sensitivity, and we compare our simulation and analytical results. This comparison validates the simulation procedures. In addition, the simple analytical equation can be used to do the initial design of future experiments before carrying out detailed simulations with the most promising parameters.

2. Simulation results and analysis

In this section, we review the work in [30]. Figure 1 displays the cross section of a negative curvature optical fiber with air holes that are filled with liquid. The glass is represented by gray regions, and the liquid is represented by blue regions. In our simulation, the core diameter, D_{core}, the gap between tubes, g, the wall thickness of cladding tubes, t, and the number of tubes, p, are set to 30 μm, 6 μm, 2 μm, and 6, respectively. This fiber transmits light at visible and near-infrared wavelengths. We selected these parameters based on previous experimental and theoretical results [28,31–33].

We calculate the fiber modes and their propagation constants using Comsol Multiphysics, a commercial full-vector mode solver based on the finite-element method. Anisotropic, perfectly matched layers (PMLs) are positioned outside the cladding in order to reduce the size of the simulation window [34]. The chromatic dispersion for both the silica glass material, n_G [35], and the commercial liquid material (Series AAA, $n = 1.36$) from Cargille Lab, n_L [36], is included in our simulation. The liquid has a refractive index of 1.36 when the wavelength is 0.589 μm and the temperature is 25 °C [36]. This liquid has a low-loss transparent window that covers both the visible and infrared wavelengths [36] and that matches the resonance condition for the negative curvature optical fiber sensor that we propose here. The thermal coefficient of a liquid, C_L, is defined as the ratio of the change of refractive index unit (RIU) to the change of temperature in degrees. The thermal coefficient used in our simulation is -3.41×10^{-4} RIU/ °C [36]. The thermal coefficient of the liquid is 10 times larger than that of silica, so that the change of the index of refraction for silica when we vary the temperature is negligible [2,36]. In Figs. 2(a) and 2(b), we show the effective index and leakage loss of the fundamental core mode when the wavelength ranges from 0.55 μm to 1.2 μm. The loss peaks in Fig. 2(b) correspond to the avoided crossings in Fig. 2(a). When the temperature increases, the resonant wavelengths also increase. Due to

OSA CONTINUUM

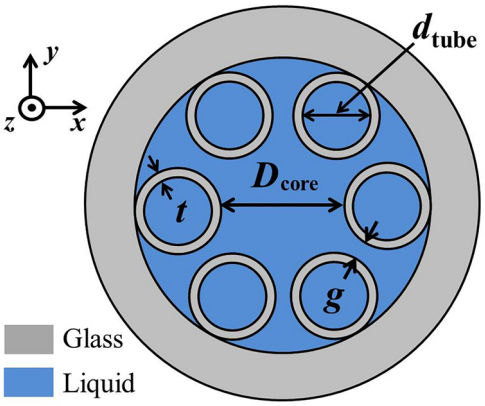

Fig. 1. Cross section of a negative curvature optical fiber filled with a liquid that is sensitive to temperature changes.

the negative value of the thermal coefficient of the liquid, the refractive index of the liquid n_L decreases, when the temperature increases. From the resonance condition, $\lambda = 2t(n_G^2 - n_L^2)^{1/2}/m$, where m represents resonance order [21], we find that the index n_L decreases, when the resonant wavelength increases, as shown in Fig. 2(b).

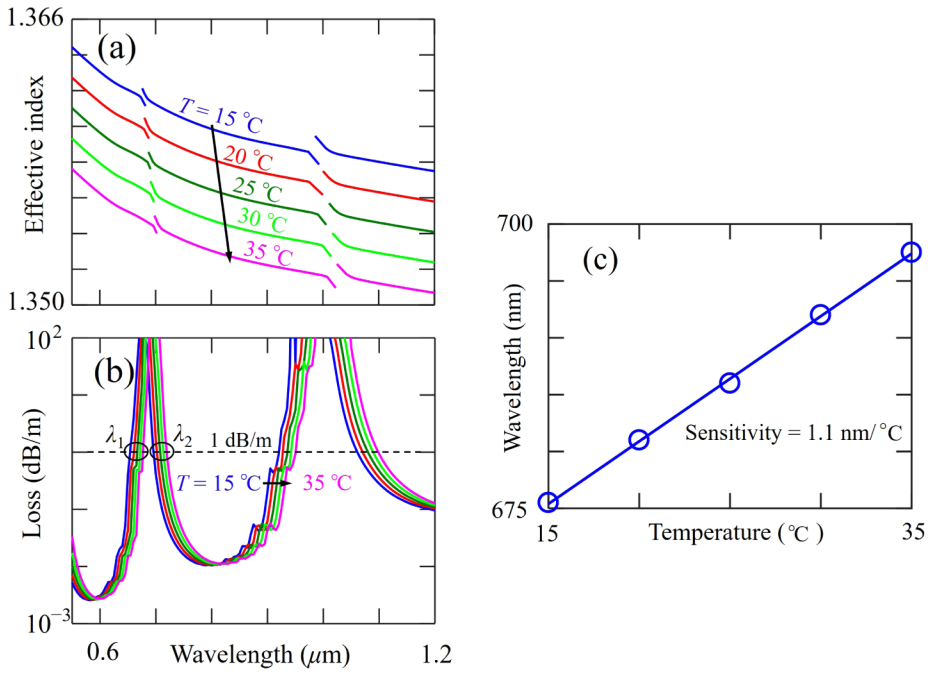

Fig. 2. (a) Effective index and (b) leakage loss of negative curvature optical fibers that are filled with liquid. The refractive index of the liquid is 1.36 when the wavelength is 0.589 μm and the temperature is 25 °C. (c) Shift of the reference wavelength of the third resonant peak, $\lambda_{ref} = (\lambda_1 + \lambda_2)/2$, when the temperature increases from 15 °C to 35 °C.

To accurately measure the increase of the resonant wavelength, we take the average of two wavelengths, $\lambda_{ref} = (\lambda_1 + \lambda_2)/2$. The wavelengths λ_1 and λ_2 correspond to the wavelengths at a

OSA CONTINUUM

loss of 1 dB/m on the both sides of the third resonant peak around 0.7 μm, as shown in Fig. 2(b). Fluctuations exist in the high-loss region during experiments [23,37]. Using the average of the wavelengths at a loss of 1 dB/m at the reference wavelength is expected to have a higher accuracy than the reference wavelength corresponding to the maximum loss. In Fig. 2(c), the blue circles show the increase of the reference wavelength of the high-loss peak, λ_{ref}, as the temperature increases, based on the simulation results from Fig. 2(b). The blue solid line shows a linear fit. Here, the slope in Fig. 2(c) corresponds to the temperature sensitivity, $d\lambda/dT$, which is defined as the ratio of change in wavelength to the change in temperature. The temperature sensitivity is 1.1 nm/°C.

In addition, the proposed device can also be used for index sensing. If we divide the temperature sensitivity of 1.1 nm/°C by the thermal coefficient of -3.41×10^{-4} RIU/°C, we find a refractive index sensitivity of -3.23×10^{3} nm/RIU for our proposed device.

3. Temperature sensitivity using liquids with different refractive indices

We now investigate the temperature sensitivity, $d\lambda/dT$, when different liquids with different refractive indices are used. In Fig. 3(a), the blue crosses show the thermal coefficient, C_L, for the liquid with refractive indices ranging from 1.30 to 1.42. All these refractive index values are measured when the wavelength is 0.589 μm and the temperature is 25 °C [36]. In our numerical simulation and analytical calculation, liquid Series AAA from Cargille Lab covers refractive indices from 1.300 to 1.395, and liquid Series AA from Cargille Lab covers refractive indices from 1.400 to 1.458 [36]. Different liquid compositions have different thermal coefficients. Because different materials have to be used to obtain different refractive index ranges [36], there is a discontinuity in the thermal coefficient between the refractive indices of 1.38 and 1.40 in Fig. 3(a). For the liquids with a refractive index from 1.30 to 1.38, their composition is perfluorocarbon and chlorofluorocarbon [36]. For the liquids with a refractive index from 1.40 to 1.42, their composition is siloxane and aliphatic [36]. We carried out the same simulation steps as in the previous section. In Fig. 3(a), red circles show the resonant wavelengths of the high-loss peaks at 25 °C for liquids with different refractive indices. The resonant wavelength decreases from 850 nm to 430 nm as the refractive index of the liquid changes from 1.30 to 1.42. Using the same procedure that we described in the previous section to track the resonant wavelength as the temperature changes, we find the temperature sensitivity for liquids with different refractive indices, indicated with red circles in Fig. 3(b). The temperature sensitivity can be improved from

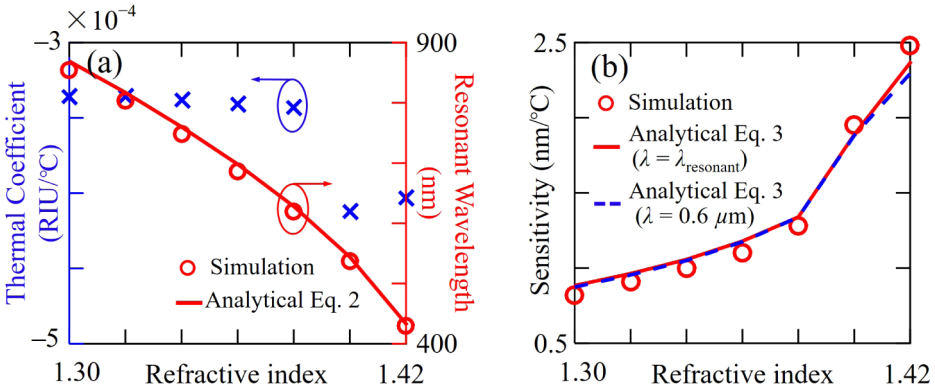

Fig. 3. (a) Thermal coefficient of liquids with different refractive indices and resonant wavelengths for negative curvature optical fibers filled with liquids that have different refractive indices. (b) Temperature sensitivity of negative curvature optical fibers filled with liquids that have different refractive indices. The order of the resonance, m, equals 3.

OSA CONTINUUM

0.82 nm/ °C to 2.48 nm/ °C when liquids are used with a refractive index that varies from 1.30 to 1.42.

These resonant wavelengths only appear in waveguides in the antiresonance condition, and the refractive index of the liquid must be lower than the refractive index of the silica glass. When the refractive index of the liquid is higher than the refractive index of the glass, the guiding mechanism becomes total internal reflection, and these resonant peaks disappear.

There are also noticeable ripples on the short wavelength side of the loss curve in Fig. 2(b). Once a fiber is made, one can always find a reference loss value away from these ripples to accurately quantify the reference wavelength, which can then be used to track the increase of the reference wavelength corresponding to the high-loss peak.

4. Comparison between simulation and analytical results

In this section, we compare the simulation results with the results of an analytical formula that we now derive. We begin with the resonance condition [21,38,39],

$$\lambda = \frac{2t\sqrt{n_G^2 - n_L^2}}{m}. \tag{1}$$

Using Eq. 1, we plot the resonant wavelength, shown by the red curve in Fig. 3(a), which agrees well with the simulation results, shown by red circles. From Eq. 1, we now obtain

$$d\lambda = \frac{-2tn_L}{m\sqrt{n_G^2 - n_L^2}} dn_L. \tag{2}$$

Using the definition of the thermal coefficient of a liquid, $dn_L = C_L dT$, we obtain the temperature sensitivity of the resonance,

$$\frac{d\lambda}{dT} = \frac{-2tn_L C_L}{m\sqrt{n_G^2 - n_L^2}}. \tag{3}$$

The absolute value of the temperature sensitivity, $d\lambda/dT$, is proportional to the thickness of the glass tube, t, the refractive index of the liquid, n_L, and the thermal coefficient, C_L; $d\lambda/dT$ is also inversely proportional to the order of the resonance, m, and the difference between the refractive index of glass, n_G, and the refractive index of the liquid, n_L. Using the refractive indices of the glass and liquid at different resonant wavelengths, shown in Fig. 3(a), along with the corresponding thermal coefficients, we can use Eq. 3 to calculate the temperature sensitivity. The result is indicated by the red solid curve in Fig. 3(b). Additionally, to simplify the calculation without considering dispersion, we also calculate the temperature sensitivity using the refractive index value of glass and the liquid at a fixed wavelength of 0.6 μm, as indicated by blue dashed curve in Fig. 3(b). All the sensitivity values using simulation results and the analytical equation with and without dispersion effects agree well, showing that dispersion does not significantly affect the sensitivity.

We also study the performance of temperature sensor using the second resonance, where $m = 2$ in Eq. 3, near the wavelength of 1.0 μm shown in Fig. 2(b). We carry out the same analysis to find the temperature sensitivity. Figure 4 shows the temperature sensitivity, $d\lambda/dT$, which changes from 1.3 nm/ °C to 3.4 nm/ °C when the refractive index of liquid changes from 1.30 to 1.42. To compare the difference between the temperature sensitivities using different resonance orders, we also include the results from Fig. 3(b). The temperature sensitivity using the second resonance is 38% higher than the temperature sensitivity using the third resonance. Equation 3 also shows that using a lower order of resonance m leads to a higher sensitivity.

Previously studied liquid-filled temperature sensors using fiber interferometers [5,7], long period fiber gratings [11], and coupled fiber structures [2], have sensitivities of 0.35 nm/ °C to

OSA CONTINUUM

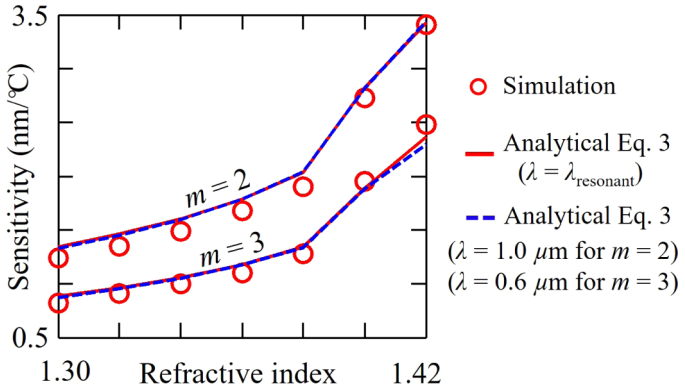

Fig. 4. Temperature sensitivity of negative curvature optical fibers filled with liquids that have different refractive indices. We show the sensitivity of the $m = 2$ and $m = 3$ resonance orders.

11.6 nm/°C. The hole sizes are only a few microns in these structures. The relatively big air core and tube diameters of 50 μm–100 μm [21,22] of negative curvature optical fibers are expected to make it easier to fill the device with liquid than is the case in photonic crystal fibers, which were used in other designs [2,5–7,10,11,15,16]. In addition, the proposed sensor does not require any special processing, such as selective filling of specific holes with liquid or inscription of fiber gratings. In Table 1, we show a comparison of different fiber temperature sensors.

Table 1. Performance comparison between different fiber temperature sensors.

	Sensitivity	Mechanism for temperature sensing	Liquid infiltration	Smallest air-hole diameter
Ref. [2]	11.61 nm/°C	Modes coupling	A single hole	3.6 μm
Ref. [5]	6.6 nm/°C	Sagnac interferometer	All holes	3.2 μm
Ref. [7]	0.35 nm/°C	Mode interference	All holes	3.0 μm
Ref. [11]	1.58 nm/°C	Long period grating	All holes	3.5 μm
This paper	2.48 nm/°C	Resonance in negative curvature fibers	All holes	14.0 μm

5. Conclusions

In conclusion, we computationally and analytically study a fiber temperature sensor that uses liquid-filled negative curvature optical fibers. When the temperature increases, the wavelength of the high-loss resonant peak also increases. The temperature sensitivity can be enhanced by using a liquid with a higher refractive index. The temperature sensitivity, $d\lambda/dT$, increases from 0.82 nm/°C to 2.48 nm/°C when the third fiber resonance and liquids with a refractive index from 1.30 to 1.42 are used. The temperature sensitivity can be further increased by 38% by using the second-order fiber resonance. The temperature sensitivity can be predicted using a simple analytical formula, whose results agree well with the simulation results. The large core and tube diameters should make the infiltration procedure easier and faster compared with solid-core photonic crystal fibers. This temperature sensor only uses a regular negative curvature optical fiber without any special post-processing, such as liquid filling of selected air holes or inscription of fiber gratings. This simple temperature sensor based on liquid-filled negative curvature optical fibers can also be applied as a refractive-index sensor or a tunable filter.

OSA CONTINUUM

Funding

National Science Foundation (NSF) (ECCS-1809622); U.S. Naval Research Laboratory (NRL) (N00173-15-1-G905).

References

1. B. T. Kuhlmey, B. J. Eggleton, and D. K. C. Wu, "Fluid-filled solid-core photonic bandgap fibers," J. Lightwave Technol. **27**(11), 1617–1630 (2009).
2. D. K. C. Wu, B. T. Kuhlmey, and B. J. Eggleton, "Ultrasensitive photonic crystal fiber refractive index sensor," Opt. Lett. **34**(3), 322–324 (2009).
3. B. Lee, "Review of the present status of optical fiber sensors," Opt. Fiber Technol. **9**(2), 57–79 (2003).
4. R. T. Bise, R. S. Windeler, K. S. Kranz, C. Kerbage, B. J. Eggleton, and D. J. Trevor, "Tunable photonic band gap fiber," in *Optical Fiber Communication Conference (OFC)*, Vol. 70 (2002), p. 466.
5. W. W. Qian, C. L. Zhao, S. L. He, X. Y. Dong, S. Q. Zhang, Z. X. Zhang, S. Z. Jin, J. T. Guo, and H. F. Wei, "High-sensitivity temperature sensor based on an alcohol-filled photonic crystal fiber loop mirror," Opt. Lett. **36**(9), 1548–1550 (2011).
6. X. Zheng, Y. Liu, Z. Wang, T. Han, C. Wei, and J. Chen, "Transmission and temperature sensing characteristics of a selectively liquid-filled photonic-bandgap-fiber-based Sagnac interferometer," Appl. Phys. Lett. **100**(14), 141104 (2012).
7. W. Qian, C. L. Zhao, C. C. Chan, L. Hu, T. Li, W. C. Wong, P. Zu, and X. Dong, "Temperature sensing based on ethanol-filled photonic crystal fiber modal interferometer," IEEE Sens. J. **12**(8), 2593–2597 (2012).
8. V. Bhardwaj, R. K. Gangwar, and V. K. Singh, "Silicone rubber-coated highly sensitive optical fiber sensor for temperature measurement," Opt. Eng. **55**(12), 126107 (2016).
9. V. Bhardwaj and V. K. Singh, "Study of liquid sealed no-core fiber interferometer for sensing applications," Sens. Actuators, A **254**, 95–100 (2017).
10. P. S. Westbrook, B. J. Eggleton, R. S. Windeler, A. Hale, T. A. Strasser, and G. L. Burdge, "Cladding mode resonances in hybrid polymer-silica microstructured optical fiber gratings," IEEE Photonics Technol. Lett. **12**(5), 495–497 (2000).
11. P. Steinvurzel, E. D. Moore, E. C. Magi, and B. J. Eggleton, "Tuning properties of long period gratings in photonic bandgap fibers," Opt. Lett. **31**(14), 2103–2105 (2006).
12. L. Shao, Z. Liu, J. Hu, D. Gunawardena, and H. Y. Tam, "Optofluidics in microstructured optical fibers," Micromachines **9**(4), 145 (2018).
13. F. M. Cox, A. Argyros, and M. C. J. Large, "Liquid-filled hollow core microstructured polymer optical fiber," Opt. Express **14**(9), 4135–4140 (2006).
14. X. Zheng, B. Debord, L. Vincetti, B. Beaudou, F. Gérôme, and F. Benabid, "Fusion splice between tapered inhibited coupling hypocycloid-core Kagome fiber and SMF," Opt. Express **24**(13), 14642–14647 (2016).
15. Y. Wang, M. Yang, D. N. Wang, and C. R. Liao, "Selectively infiltrated photonic crystal fiber with ultrahigh temperature sensitivity," IEEE Photonics Technol. Lett. **23**(20), 1520–1522 (2011).
16. D. Hu, J. Lim, Y. Cui, K. Milenko, Y. Wang, P. Shum, and T. Wolinski, "Fabrication and characterization of a highly temperature sensitive device based on nematic liquid crystal filled photonic crystal fiber," IEEE Photonics J. **4**(5), 1248–1255 (2012).
17. Y. Wang, C. R. Liao, and D. N. Wang, "Femtosecond laser-assisted selective infiltration of microstructured optical fibers," Opt. Express **18**(17), 18056–18060 (2010).
18. L. Xiao, W. Jin, M. S. Demokan, H. L. Ho, Y. L. Hoo, and C. Zhao, "Fabrication of selective injection microstructured optical fibers with a conventional fusion splicer," Opt. Express **13**(22), 9014–9022 (2005).
19. Y. Wang, F. Couny, P. J. Roberts, and F. Benabid, "Low loss broadband transmission in optimized core-shape Kagome hollow-core PCF," in *Conference on Lasers and Electro-Optics 2010*, OSA Technical Digest (CD) (Optical Society of America, 2010), paper CPDB4.
20. Y. Y. Wang, N. V. Wheeler, F. Couny, P. J. Roberts, and F. Benabid, "Low loss broadband transmission in hypocycloid-core Kagome hollow-core photonic crystal fiber," Opt. Lett. **36**(5), 669–671 (2011).
21. C. Wei, R. J. Weiblen, C. R. Menyuk, and J. Hu, "Negative curvature fibers," Adv. Opt. Photonics **9**(3), 504–561 (2017).
22. F. Yu and J. C. Knight, "Negative curvature hollow-core optical fiber," IEEE J. Sel. Top. Quantum Electron. **22**(2), 146–155 (2016).
23. F. Poletti, "Nested antiresonant nodeless hollow core fiber," Opt. Express **22**(20), 23807–23828 (2014).
24. F. Meng, B. Liu, Y. Li, C. Wang, and M. Hu, "Low loss hollow-core antiresonant fiber with nested elliptical cladding elements," IEEE Photonics J. **9**(1), 1–11 (2017).
25. A. M. Cubillas, X. Jiang, T. G. Euser, N. Taccardi, B. J. M. Etzold, P. Wasserscheid, and P. St. J. Russell, "Photochemistry in a soft-glass single-ring hollow-core photonic crystal fiber," Analyst **142**(6), 925–929 (2017).
26. C. Wei, C. R. Menyuk, and J. Hu, "Bending-induced mode non-degeneracy and coupling in chalcogenide negative curvature fibers," Opt. Express **24**(11), 12228–12239 (2016).

OSA CONTINUUM

27. B. Debord, A. Amsanpally, M. Chafer, A. Baz, M. Maurel, J. M. Blondy, E. Hugonnot, F. Scol, L. Vincetti, F. Gérôme, and F. Benabid, "Ultralow transmission loss in inhibited-coupling guiding hollow fibers," Optica **4**(2), 209–217 (2017).
28. X. Liu, W. Ding, Y. Y. Wang, S. Gao, L. Cao, X. Feng, and P. Wang, "Characterization of a liquid-filled nodeless anti-resonant fiber for biochemical sensing," Opt. Lett. **42**(4), 863–866 (2017).
29. F. Giovanardi, A. Cucinotta, and L. Vincetti, "Inhibited coupling guiding hollow fibers for label-free DNA detection," Opt. Express **25**(21), 26215–26220 (2017).
30. C. Wei, J. T. Young, C. R. Menyuk, and J. Hu, "Temperature sensor using fluid-filled negative curvature fibers," in *Conference on Lasers and Electro-Optics*, OSA Technical Digest (online) (Optical Society of America, 2018), paper JW2A.179.
31. M. Michieletto, J. K. Lyngsø, C. Jakobsen, J. Lægsgaard, O. Bang, and T. T. Alkeskjold, "Hollow-core fibers for high power pulse delivery," Opt. Express **24**(7), 7103–7119 (2016).
32. C. Wei, C. R Menyuk, and J. Hu, "Impact of cladding tubes in chalcogenide negative curvature fibers," IEEE Photonics J. **8**(3), 1–9 (2016).
33. P. Uebel, M. C. Günendi, M. H. Frosz, G. Ahmed, N. N. Edavalath, J.-M. Ménard, and P. St. J. Russell, "Broadband robustly single-mode hollow-core PCF by resonant filtering of higher-order modes," Opt. Lett. **41**(9), 1961–1964 (2016).
34. K. Saitoh and M. Koshiba, "Leakage loss and group velocity dispersion in air-core photonic bandgap fibers," Opt. Express **11**(23), 3100–3109 (2003).
35. I. H. Malitson, "Interspecimen comparison of the refractive index of fused silica," J. Opt. Soc. Am. **55**(10), 1205–1209 (1965).
36. Cargille Labs, "Refractive Index (Matching) Liquids," http://www.cargille.com/refractivestandards.shtml.
37. B. Debord, M. Alharbi, T. Bradley, C. Fourcade-Dutin, Y. Y. Wang, L. Vincetti, F. Gérôme, and F. Benabid, "Hypocycloid-shaped hollow core photonic crystal fiber Part I: Arcs curvature effect on confinement loss," Opt. Express **21**(23), 28597–28608 (2013).
38. C. Wei, R. A. Kuis, F. Chenard, C. R. Menyuk, and J. Hu, "Higher-order mode suppression in chalcogenide negative curvature fibers," Opt. Express **23**(12), 15824–15832 (2015).
39. J. L. Archambault, R. J. Black, S. Lacroix, and J. Bures, "Loss calculations for antiresonant waveguides," J. Lightwave Technol. **11**(3), 416–423 (1993).